Research Article Vol. 33, No. 5 / 10 Mar 2025 / Optics Express 9199
Optics EXPRESS

Compact extended-DOF microscope through electrowetting lens

ESTELA ESPAÑOL, ANGEL TOLOSA, GENARO SAAVEDRA, MANUEL MARTINEZ-CORRAL, AND NICOLO INCARDONA*

3D Imaging and Display Laboratory, Department of Optics, Universitat de València, 46100 Burjassot, Spain
*nicolo.incardona@uv.es

Abstract: In optical microscopy, the intrinsic trade-off between resolution and depth of field (DOF) prevents the observation of 3D samples, limiting the observable thickness to some micrometers. The usual solution to this problem is to mechanically scan the object in depth. However, this slows down the process and can induce vibrations in soft samples. To overcome these drawbacks, we propose the use of an electrically tunable lens (ETL) based on electrowetting effect. Specifically, we propose an extended-DOF microscope set up in a very compact architecture in which full telecentricity is no longer achieved. On top of that, the axial scanning is carried out by the non-afocal coupling between two M12 lenses and the ETL. The main feature of the proposed extended-DOF microscope is that, despite its compactness, it can capture stacks of images with long depth range, constant magnification and a spatial resolution that equals that of the standard microscope and remains invariant along the depth range. We also show that the proposed idea can be implemented as an add-on attachable to any commercial microscope, which enables the use of all the microscope facilities.

1. Introduction

Nowadays, imaging thick 3D samples is widely used in those fields where visualizing small complex structures is crucial. Optical microscopy is highly demanded for material engineering, clinical research and biomedical applications, among others. In fact, optical microscopes allow to resolve fine details of a sample. Nevertheless, the axial extension of a specimen that can be imaged with high resolution, the so-called depth of field (DOF), is limited to some micrometers. To observe a sample whose thickness exceeds this depth, it is thus necessary to carry out an axial scanning.

A simple solution to this problem is to perform a mechanical scanning, in order to change the focused portion of the sample. However, mechanical displacement subsequent effects, such as vibrations and inertia, require a brief stabilization period, which slows down the capture process. Additionally, they difficult the use of immersion objectives. Several methods have been proposed to overcome the limitations of mechanical displacement of the sample [1], such as the use of moving mirrors [2,3], deformable mirrors [4], or the insertion of a phase mask [5] or a z-splitter prism [6] to extend the DOF. Fast scanning alternatives include the use of electrically tunable lenses (ETL), spherical lenses whose face curvature, and therefore focal length, can be changed by varying the voltage applied. The insertion of an ETL allows to perform an axial scanning of the sample without mechanical movements. This characteristic makes it a cheap and convenient solution to obtain an extended DOF (EDOF), retaining the resolution across a depth range several times greater than the native DOF.

The performances of the diverse scanning systems based on ETLs depend on the design and allocation of the optical components. In [7] and [8], the ETL is placed at a certain distance from the microscope objective. For both works, the results show that the magnification and resolution obtained are not constant. Furthermore, the relation between the control current of

#546143 https://doi.org/10.1364/OE.546143
Journal © 2025 Received 25 Oct 2024; revised 6 Jan 2025; accepted 22 Jan 2025; published 24 Feb 2025

Optics EXPRESS

the ETL and the object plane shift is not linear. In [9] and [10], the ETL is placed attached to the objective, to be as close as possible to its aperture stop, which is usually located inside the objective. Not placing the ETL right at the aperture stop plane causes the magnification to slightly change when the ETL focal length changes. Additionally, as commercial ETLs usually have clear apertures smaller than the diameter of the aperture stop, the effective numerical aperture of the objective is reduced, leading to a loss of resolution with respect to the native microscope. Other systems include the use of one or multiple varifocal lenses to perform continuous scanning and zoom [11–13]. These systems can achieve good results, but they are expensive and difficult to manufacture and control. Besides widefield microscopy, ETLs have also been included in 3D systems such as confocal and lightsheet microscopes [14,15], among others. On the other hand, less simple solutions include the use of acousto-optic components [16] and spatial light modulators [17].

To overcome the limitations on the ETL clear aperture and location, in a previous work published by our group, an afocal relay was used to conjugate the aperture stop with the ETL [18]. The system was mounted on the optical bench, in double-telecentric configuration. In [19], the same optical system is used and combined with speckle illumination, to obtain super-resolved images with EDOF. Also in [20], an ETL is conjugated with the aperture stop to obtain EDOF. In this case, the system was built harnessing the lateral port of a commercial microscope. It must be noted that the system's overall length introduces significant complexity in the alignment process. This is a critical point, as minor misalignments on the setup might result in lateral displacement between consecutive images of the captured stack.

In this work, we propose a compact EDOF microscope, based on the insertion of an ETL at the exit pupil plane. The system captures a stack of images, each one focused at a different depth, by varying the optical power of the ETL. We avoid double-telecentric configuration, with the aim of facilitating the alignment of the system: the tube lens is placed as close as possible to the microscope objective, to shorten the length of the system. Additionally, we make use of M12 lenses for the second relay system, as they are cost-effective and provide good optical quality even with short focal length. We demonstrate that the system achieves constant lateral resolution for the entire scanning range. Afterwards, we build an add-on attachable to the camera port of a commercial microscope. We thus demonstrate that it is possible to convert a commercial microscope into an EDOF microscope through a simple, portable and cost-effective add-on, composed by the M12 lenses relay, the ETL and the camera. With this device, it is possible to capture 3D images of thick samples, harnessing all the microscope facilities. We finally show the images of 3D samples captured with this system, with different illumination techniques. Consequently, we demonstrate both the 3D imaging capability of the device and its versatility. In fact, the add-on can be used with all microscopy techniques available in the host microscope, such as brightfield, darkfield, fluorescence and phase contrast microscopy.

2. Materials and methods

Modern optical microscopes can be schematized as the coupling between an infinity-corrected microscope objective and a converging tube lens. An optical scheme is shown in Fig. 1. The objective is designed to be telecentric in the object space. This means that the entrance pupil is at the infinity, what is achieved by placing the aperture stop at the back focal plane. The objective collects the light proceeding from the sample and sends its image to the infinity. The tube lens focuses this image onto the digital camera sensor, which is placed at its back focal plane.

The aim of optical microscopes is to provide high-resolution images of the sample under observation. The resolution limit, ρ, of the system is given by this formula [21]:

$$\rho = \frac{\lambda}{2\mathrm{NA}} + \frac{\delta}{M}, \tag{1}$$

Optics EXPRESS

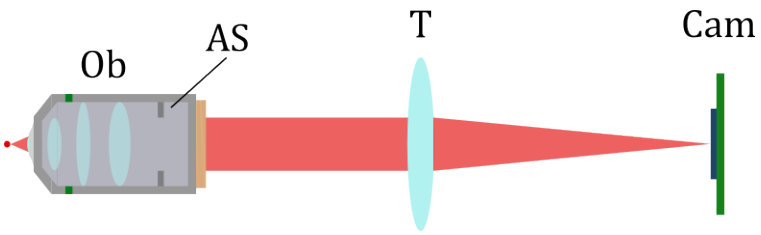

Fig. 1. Scheme of an optical microscope. Ob is the microscope objective and *AS* is its aperture stop. The tube lens, *T*, focuses the light onto the sensor of the digital camera, *Cam*.

where λ is the wavelength of the light emitted or scattered by the sample, NA is the numerical aperture of the objective, δ is the pixel size of the camera and M is the magnification of the microscope (calculated as $M = f_T/f_{ob}$, f_{ob} standing for the objective focal length and f_T for the tube lens one). For microscopes equipped with high-magnification objective, the resolution is mainly determined by the NA, which can be approximated to the simple relation:

$$\mathrm{NA} = \frac{\Phi_{AS}}{2f_{ob}}, \tag{2}$$

where Φ_{AS} is the aperture stop diameter.

Another important feature of the microscope is its DOF, which is the length of the axial range of the sample whose image has a resolution similar to that of the object plane (the plane conjugated with the sensor). Specifically, the limits of the DOF are defined as the depths at which the resolution limit increases by a factor of $\sqrt{2}$ compared to its value at the object plane. The value is calculated as

$$DOF = \frac{\lambda}{\mathrm{NA}^2} + \frac{\delta}{M \cdot \mathrm{NA}}. \tag{3}$$

There is, thus, a trade-off between the resolution and the DOF provided by the microscope. To obtain high resolution (i.e. low resolution limit), a high-NA objective is needed, which leads to small DOF (typically limited to some micrometers). This effect is indeed undesirable when imaging a thick sample. In such case, only a thin slice is focused sharply and the rest of the sample is imaged with strong blur. This blur affects the contrast of the acquired 2D image, and its final influence depends on the type of the sample.

In order to obtain a high-resolution 3D image of a thick sample, it is thus necessary to perform an axial scanning across all the sample depth, while acquiring a 2D image at every scanning step. In this work, we make use of an ETL, a lens whose focal length can be controlled by simply applying a voltage, for tuning the object-plane position. In this way, it is possible to scan the sample along the axial direction without mechanical movements.

It is known that in case of a double-telecentric microscope, placing the ETL in the aperture stop plane allows the capture of image stacks with constant magnification and resolution [18]. Double-telecentric means that both the entrance and the exit pupils are at the infinity. In a microscope, double-telecentric condition is achieved by placing the objective and the tube lens in afocal configuration. That is, with the front focal plane of the tube lens matching the back focal plane of the objective (in which the aperture stop is located). However, this is not the case of commercial microscopes, which are set up with the tube lens close to the objective, aiming to achieve a more compact design.

3. Telecentricity analysis

At this point, it is necessary to analyse the impact of the lack of telecentricity on the resolution and magnification. To perform the analysis in an easy way, we take advantage of ABCD matrix

Optics EXPRESS

formalism [22]. This geometrical formalism assumes the paraxial approximation, but avoids considering the limited size of optical elements. As for the wave-optics approach, it is also based on the paraxial approximation (when Fresnel equations are used), but the limited size of elements is the key parameter. However, when one intends to calculate the image position and conjugation relations, both approaches provide similar results, so wave optics calculations are not necessary. In fact, the wave-optics image is the same as the geometrical image but convolved with the PSF, which derives from the wave behavior. According to the ABCD, the propagation of light beams from the object plane to the sensor plane can be computed by the product in cascade of several 2x2 matrices, each corresponding to a different propagation step.

To perform the matrix computation we follow the scheme shown in Fig. 2, where we assume that the ETL is set at the aperture stop plane, preceeding the tube lens at a distance d from that plane. We also consider that the object is not at the front focal plane of the objective, but at an arbitrary distance x_0. Taking this into account, we can write

$$\mathbf{M}_{sys} = \mathbf{P}_{T-C} \times \mathbf{R}_T \times \mathbf{P}_{L-T} \times \mathbf{R}_L \times \mathbf{M}_{F_{ob}-F'_{ob}} \times \mathbf{P}_{O-F_{ob}}. \tag{4}$$

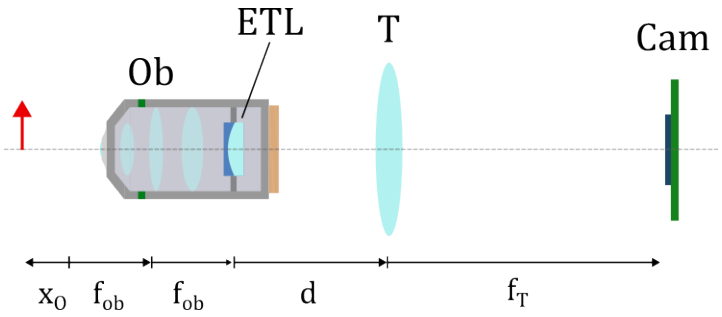

Fig. 2. Scheme of the microscope with the ETL inserted in the aperture stop. The ETL's function is to collimate the beam proceeding from the objective when the object is shifted from its front focal plane. The red arrow represents the object, shifted a distance x_0. From this scheme, the magnification of the system and the conjugation relation are derived through ray transfer matrix analysis.

Here, $\mathbf{M}_{sys}$ is the matrix that describes the entire system. Matrix $\mathbf{P}_{O-F_{ob}}$ accounts for the free-space propagation between the object position and the objective front focal plane. Matrices $\mathbf{P}_{L-T}$ and $\mathbf{P}_{T-C}$ account, respectively, for free-space propagation between the tunable lens (L) and the tube lens (T), and between the tube lens and the camera (C). Additionally, $\mathbf{R}_T$ and $\mathbf{R}_L$ are the matrices that account for the refraction in the tube lens and the tunable lens. Finally, $\mathbf{M}_{F_{ob}-F'_{ob}}$ is the matrix that links the front and the back focal planes of the objective. Subsequently, we express this equation in an explicit form:

$$\begin{aligned}\mathbf{M}_{sys} = \begin{bmatrix} A & B \\ C & D \end{bmatrix} &= \begin{bmatrix} 1 & -f_T \\ 0 & 1 \end{bmatrix} \begin{bmatrix} 1 & 0 \\ P_T & 1 \end{bmatrix} \begin{bmatrix} 1 & -d \\ 0 & 1 \end{bmatrix} \begin{bmatrix} 1 & 0 \\ P_L & 1 \end{bmatrix} \begin{bmatrix} 0 & -f_{ob} \\ P_{ob} & 0 \end{bmatrix} \begin{bmatrix} 1 & x_0 \\ 0 & 1 \end{bmatrix} = \\ &= \begin{bmatrix} -f_T P_{ob} & f_{ob} f_T P_L - f_T P_{ob} x_0 \\ P_{ob}\,(1 - dP_T) & -f_{ob}\,[P_T\,(1 - dP_L) + P_L] + P_{ob}\,(1 - dP_T)\,x_0 \end{bmatrix}.\end{aligned} \tag{5}$$

Here P stands for optical power, defined as inverse of the focal length ($P = 1/f$). According to ABCD formalism, by setting the element $B = 0$ and solving the equation, we get the conjugation

Optics EXPRESS

relation, that is, the object plane that is imaged at the camera plane. This corresponds to the value

$$x_0 = f_{ob}^2 P_L. \tag{6}$$

From this equation we find that, as expected, when $P_L = 0$ the object plane is set just at the objective front focal plane ($x_0 = 0$). On the contrary, the object plane is shifted towards the objective when P_L is positive (converging lens), and in the opposite direction when negative. In fact, positive values of x_0 correspond to the left-to-right direction, while negative values correspond to the right-to-left direction (like in Fig. 2).

An additional insight derived from the entire matrix is that, provided that the conjugation occurs, the element A of the matrix accounts for the lateral magnification, M_0, so that

$$M_0 = -\frac{f_T}{f_{ob}}. \tag{7}$$

This is the classic formula for the microscope magnification, but the important point is that it is obtained here to be independent from the value of x_0. Thus, it is demonstrated that, to meet the challenge of capturing stacks of microscopy images with constant magnification, and therefore resolution, it is not necessary to use a double-telecentric configuration, but it is rather sufficient to have telecentricity in the object space.

As is known, the aperture stop is located inside the objective. Therefore, in a laboratory experiment it is not easy to place the ETL right at the aperture stop. Another problem comes from the fact that the ETL effective aperture may be smaller than the stop diameter. This scenario can have a doubly detrimental effect. First, the numerical aperture of the system would be reduced. On the other hand, the use of the outermost parts of the ETL can reinforce the effect of optical aberrations.

The straightforward solution is to use a relay and insert the ETL at a plane conjugated to the aperture stop. As the objective and the tube lens are not in afocal configuration, the exit pupil is not at the back focal plane of $L1$ (see Fig. 3), but shifted a distance y given by

$$y = \left(\frac{f_1}{f_T}\right)^2 (f_T - d). \tag{8}$$

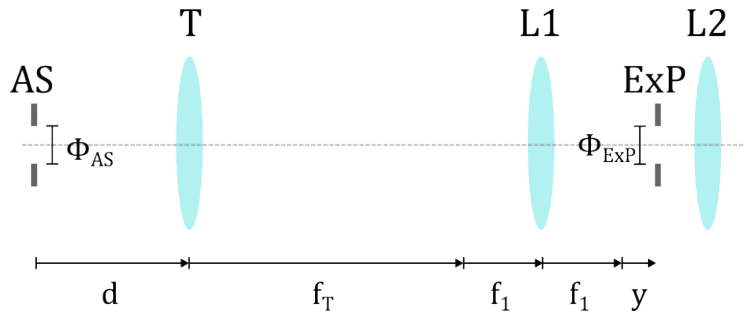

Fig. 3. The scheme to derive the exit pupil position when the microscope is not double telecentric. $L1$ and $L2$ are the lenses of the afocal relay, and T and $L1$ are coupled afocally. If the tube lens is placed close to the objective, the exit pupil is shifted further from $L1$, by a distance y.

The scheme of the complete system is shown in Fig. 4(a). Again, we can calculate the ABCD matrix, $\mathbf{M}_T$, corresponding to this total system

$$\mathbf{M}_T = \mathbf{M}_{F_1 - F_2'} \times \mathbf{M}_{F_{ob} - F_T'} \times \mathbf{P}_{O - F_{ob}}. \tag{9}$$

Optics EXPRESS

It is straightforward to find that

$$\mathbf{M}_{F_{ob}-F'_T} = \begin{bmatrix} -f_T P_{ob} & 0 \\ P_{ob}\,(1 - dP_T) & -f_{ob} P_T \end{bmatrix} \tag{10}$$

and

$$\mathbf{M}_{F_1-F'_2} = \begin{bmatrix} -f_2 P_1 (1 - yP_L) & f_1 f_2 P_L \\ -P_1 P_2 P_L y^2 & -f_1 P_2\,(1 + yP_2) \end{bmatrix}. \tag{11}$$

Then

$$\mathbf{M}_T = \begin{bmatrix} M_E & -f_1 f_2 f_{ob} P_T P_L \\ -M_E P_T (1 - dP_T) & M_E^{-1}\left(1 + f_1^2 P_T (1 - dP_T)\right) \end{bmatrix} \begin{bmatrix} 1 & x_E \\ 0 & 1 \end{bmatrix} \tag{12}$$

where

$$M_E = \frac{f_2}{f_1}\frac{f_T}{f_{ob}}. \tag{13}$$

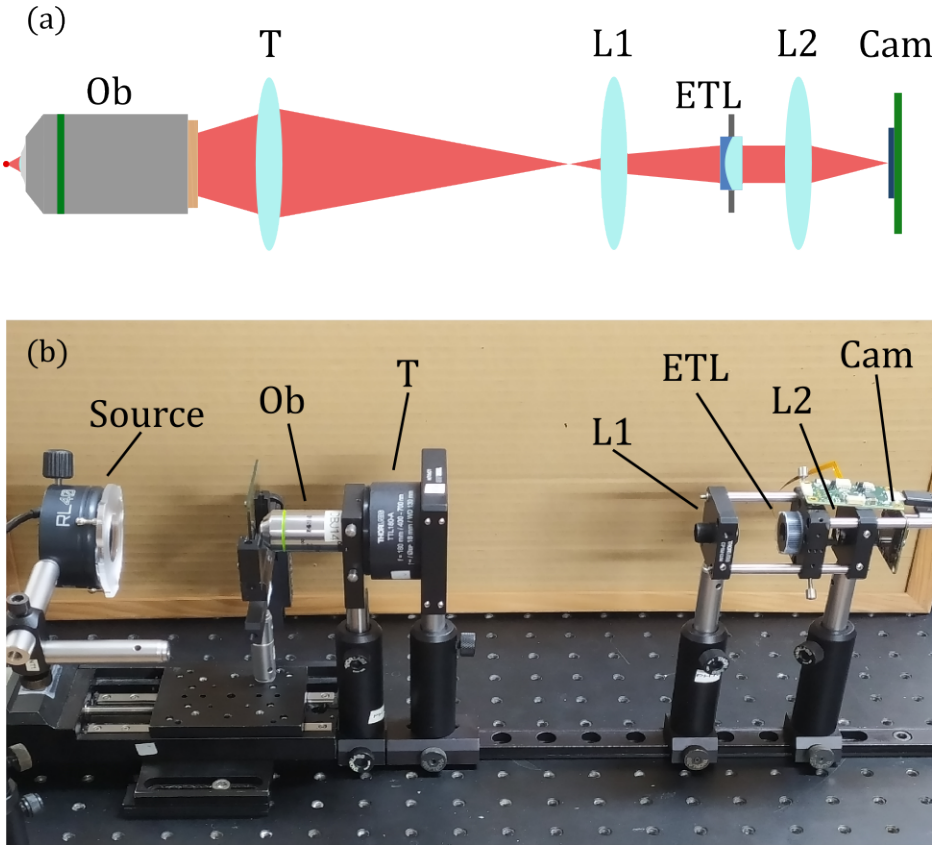

Fig. 4. (a) The full optical scheme of the EDOF microscope. The system consists of an object-space-telecentric microscope (Objective (Ob) and tube lens (T)), followed by an afocal relay ($L1$ and $L2$). Lenses T and $L1$ are coupled, also, afocally. The ETL is inserted right at the exit pupil. (b) The scanning microscope system mounted on the optical bench.

Optics EXPRESS

After performing the last matrix product, it is immediate to find that the object plane position is given by

$$x_E = \left(\frac{f_1}{f_T}\right)^2 f_{ob}^2 P_L, \tag{14}$$

and the lateral magnification is indeed equal to M_E, as defined in Eq. (13).

Another important parameter is the exit pupil diameter:

$$\Phi_{ExP} = \left(\frac{f_1}{f_T}\right) \Phi_{AS}. \tag{15}$$

As mentioned above, the clear aperture of the ETL must be bigger than Φ_{ExP}, not to compromise the lateral resolution of the microscope. Thus, an $L1$ lens with f_1 much smaller than f_T is highly recommendable.

4. Compact EDOF system

In order to reduce the overall length of the system, aiming at compactness and reduction of the impact of small misalignments, we placed the tube lens as close as possible to the objective and used short focal-length relay lenses. From our experience, typical 1-inch lenses with short focal length (f<100 mm) do not have good imaging performances. On the contrary, M12 lenses are indeed mini-objectives, which are composed by several singlets, and are characterized by having short focal lengths and good imaging capabilities. Therefore, we decided to use one pair of equal M12 lenses for the afocal relay. Note that the M12s are designed to conjugate, with a minimum impact of aberrations, a distant object with the sensor, which is placed in the back focal plane of the M12. This will be the case for the L_2 lens of our relay, but not for the L_1 lens. In the latter case, the M12 needs to conjugate its front focal plane to infinity. Thus the first M12 must be set in reverse orientation.

The optical system is shown in Fig. 4(b). We used a 20× / 0.4 objective from Olympus (PLN20×). Since it is designed for $f_T = 180$ mm, we used a tube lens provided by Thorlabs with that focal length (TTL-180A). For the relay, we chose $f_1 = f_2 = 25$ mm (M12-25-5MP from Jetsun), to get a good trade-off between the system length, scanning resolution and depth range (Eq. (14)). The second lens, $L2$, was chosen identical to $L1$ to maintain the magnification equal to that of the native microscope (Eq. (13)). If a sensor with large pixel size were used, f_2 should be chosen larger than f_1, to allow the increase of the total magnification. In this way, the influence of the pixel on the lateral resolution is reduced (Eq. (1)). The tunable lens was an A-39N from Corning. This ETL is based on electrowetting effect [23,24]. It has a clear aperture of $\Phi_L = 3.9$ mm and its optical power-voltage relation is linear in the range $P_L \in [-5,\ 15]$ D. With the components chosen and following Eq. (15), the condition Φ_{AS}<27.8 mm must be fulfilled to maintain the resolution equal to that of the native microscope. This condition is met by all the commercially available microscope objectives, which means that the system can work with all potential objectives.

As the tube lens was placed next to the objective, the exit pupil was shifted away from $L1$, following Eq. (8). A correct positioning of the ETL is fundamental to maintain the magnification and resolution constant while P_L changes. To experimentally place the ETL right at the exit pupil, we illuminated the objective through a diffuser and then found the position of the plane at which the sharp image of the aperture stop was obtained. Finally, the camera was a DFM 37UX250-ML (from The Imaging Source), equipped with a CMOS sensor having 2448 × 2048 pixels of side $\delta = 3.45$ μm.

The essential optical components of any commercial microscope are the objective and the tube lens. Thus, in a further step, we decided to implement the EDOF proposal in a commercial microscope by attaching the second part of the system ($L1$, ETL, $L2$ and camera) to the camera

Optics EXPRESS

port. To do so, two adjustments were needed. The first one was to adjust the position of the entire add-on to make sure that the tube lens and the lens $L1$ were coupled afocally. This adjustment was easy to realize. First, a thin sample was focused with the native microscope. After that, the add-on without the ETL was inserted in the camera port and its position was changed until the image of the thin sample appeared on focus. This ensures that the front focal plane of $L1$ matches exactly the position of the intermediate image (corresponding to the back focal plane of the tube lens). The second one was to place the ETL at the exit pupil. This adjustment was made in the same way that it was done on the optical bench. Specifically, a piece of paper was placed attached to the ETL and the objective was illuminated through a diffuser. Then, the ETL was moved until the image of the aperture stop appeared on focus on the paper.

The system mounted in a commercial microscope is shown in Fig. 5. The host microscope used was a Nikon Eclipse TE2000-U. The add-on is just ~10 cm long. This configuration has the advantage of easily exploiting all the microscope facilities, such as the illumination systems, filters, sample stage and objective turret. In fact, as will be shown in the Results section, we used it to image 3D samples with the EDOF system, with several different illumination techniques and objectives.

Fig. 5. The EDOF microscope implemented by coupling the add-on with the ETL to a commercial microscope.

Optics EXPRESS

5. Results

First of all, we conducted a series of experiments with the EDOF microscope mounted on the optical bench (Fig. 4(b)), to verify the invariance of its lateral resolution. In the first experiment, we compared the lateral resolution of the EDOF microscope with the one obtained by the same system without the ETL. To do so, we used a high-resolution target (#37-539 from Edmund Optics, with measurable resolution limit up to 304 nm), placed at the objective front focal plane.

First, we removed the ETL and captured a sharp image of the resolution target. Then, for the EDOF system, we re-inserted the ETL and we adjusted the voltage applied to this element, until we got a focused image of the object (that is, we set the V_L corresponding to $P_L = 0\ D$). The images captured are shown in Fig. 6. The insets show the highest-frequency resolvable elements with both systems. In this target, the frequency of each element is indicated in line pairs per mm (lp/mm). In Fig. 6(c), the intesity profile plots along the elements of the insets are reported and compared for both systems. The visual inspection of the images and the comparison of the intensity profiles confirm that the insertion of the ETL does not compromise the image quality.

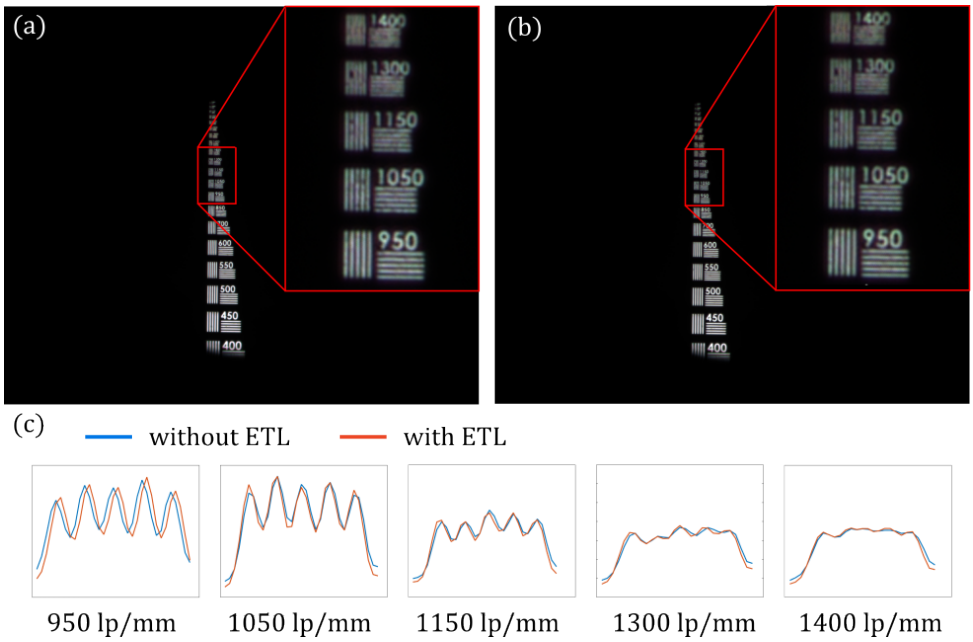

Fig. 6. The images of a high-resolution target placed at the objective front focal plane. (a) Image captured with the system without ETL. (b) Image captured with the ETL having $P_L = 0\ D$. The insets show a detail of the highest-frequency resolvable elements. (c) Comparison between the intensity profiles of both systems, at each of the frequencies of the insets.

The next experiments were to confirm that the EDOF microscope provides constant magnification and resolution across all its depth range. For this purpose, we mounted the high-resolution target onto a motorized stage. We displaced the target along the axial direction at the distances calculated through Eq. (14), varying P_L from −5 D to +15 D by means of 5 D steps. Correspondingly, we varied the voltage applied to the ETL, to control P_L. The result is shown in Fig. 7. Here, only the highest-frequency resolvable elements are reported for each image. Similarly to the previous Figure, the intensity profile plots are also reported. In this case, for each plot, the intensity obtained at each distance is reported. From the visual analysis of the images and the intensity profile plots, we could confirm that the resolution provided by the system remains

Optics EXPRESS

constant across the axial range, with a maximum resolvable frequency approximately equal to 1300 lp/mm. With the images captured in this experiment, we also calculated the system magnification at each object distance. To do so, we considered 5 frequency elements (specifically: 450, 500, 550, 600 and 700 lp/mm). As can be seen, each element consists of 9 lines (5 white lines and 4 black lines between the white ones) of equal width. We extracted the number of pixels corresponding to the 9 lines of each frequency element. Then, we multiplied the number of pixels by the pixel size, to get the size of the 9 lines in the image space, and divided this value by the corresponding size in the object space (9 times the width of a line of a specific frequency element). We calculated an average of the 5 magnifications obtained at the 5 frequency elements considered. We obtained an average magnification of $M_E = 20.46$, with maximum value of 20.50 and minimum value of 20.42. The variation between maximum and minimum values is therefore ~0.1%, which confirms the theoretical demonstration of constant magnification.

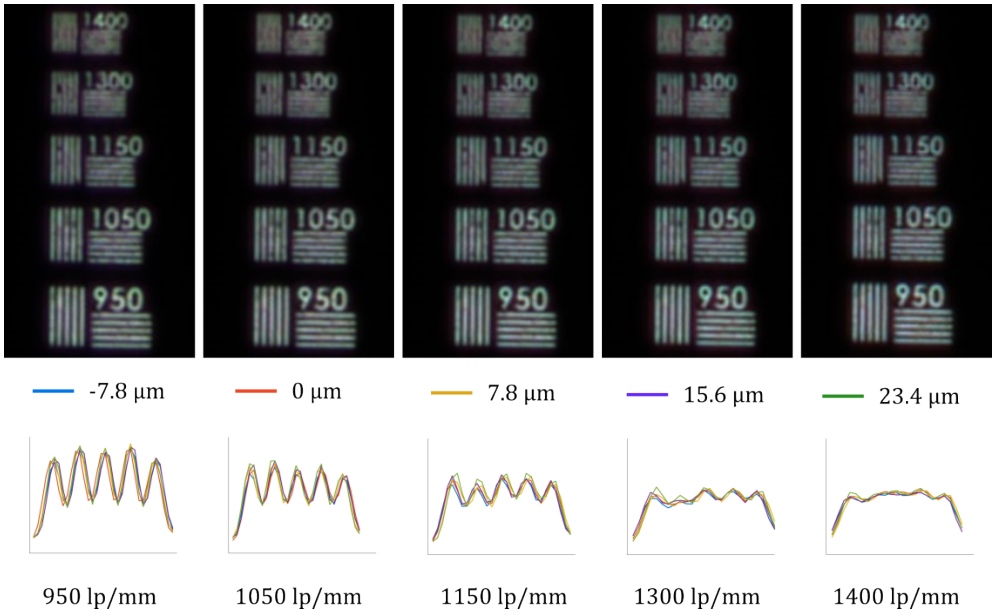

Fig. 7. Detail of the highest-frequency resolvable elements of the image of a high-resolution target placed at different distances, captured with the EDOF microscope. The distance indicated is given related to the objective front focal plane. To focus the target, P_L is set sequentially to $P_L = -5\ D,\ 0\ D, +5\ D, +10\ D, +15\ D$ by controlled tuning of the applied voltage. In the bottom line, the comparison between the intensity profiles obtained at each distance is shown, for each of the frequencies.

Finally, we conducted experiments for the quantitative analysis of the optical performances of the proposed system. For the spatial resolution, the slant edge method was used, which provides an indirect measure of the modulation transfer function (MTF) of the system from a single capture of a slant edge target (R2L2S2P from Thorlabs) [25]. Another advantage is that from the same edge target image one can obtain the MTF at different heights of the field of view (FOV). The slant edge target was mounted on the motorized stage and centered so that it passed through the optical axis of the microscope. First, we obtained the edge image with the host microscope (i.e., with the system consisting only of the objective and the tube lens). The MTFs obtained at three different heights (0%, 50% and 70% of the FOV) are shown in Fig. 8, upper left graph. This plot constitutes the ground truth of our proposal. The other five plots shown in Fig. 8 were obtained with the EDOF system, after inserting the relay and the ETL. The images

Optics EXPRESS

were captured with the edge target placed at the same distances as indicated in Fig. 7, setting $P_L = -5\ D,\ 0\ D, +5\ D, +10\ D, +15\ D$. As expected, the best results were obtained with the host microscope. However, the EDOF system provided results very close to those, over the entire depth range, specifically when considering the region of the graph where the MTF is greater than 0.1. This confirmed that EDOF preserves, basically, the spatial resolution while greatly extending the DOF.

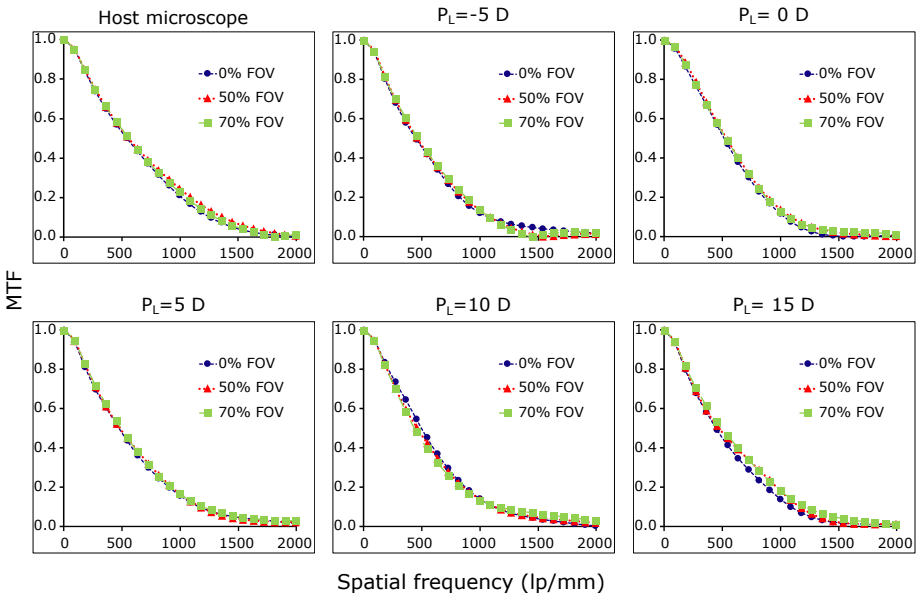

Fig. 8. The MTFs of the host microscope and of the proposed EDOF system for five different values of P_L. The MTFs have been measured at three different heights of the FOV (0%, 50% and 70%).

Concerning the FOV, in the case of the host microscope it was determined by the sensor size. In our case, the sensor measured 8.44 × 7.06 mm, and therefore the FOV as evaluated in the object space was 412 × 345 µm. In the case of the EDOF system one should expect a reduction in the FOV and also the introduction of some vignetting. To analyse this, we performed a simple experiment: we placed a blank object at the object plane of the EDOF microscope and we captured an image. Then, we averaged the intensity across several diameters of the circular FOV. The result is shown in Fig. 9. From this figure, one finds that the FOV is now circular with diameter 258 µm. The vignetting, measured as the number of pixels with an intensity that is included between the minimum and maximum divided by the total number of pixels of the FOV, affected the 15.5% of the field.

For the assessment of the 3D imaging capability of the proposed system, we used a 3D calibration target, namely the Argo-HM slide V2 from Argolight. Specifically, we observed the "Sphere" pattern, which consists of three circles of 50 µm diameter placed on three orthogonal planes, representing the equator and two meridians of a sphere. As this is a fluorescent object, it was imaged with the system shown in Fig. 5, to exploit the fluorescence illumination system of the Nikon microscope. The objective used in this case was a 20× / 0.5 from Nikon (CFI Plan Fluor 20×). The object plane was varied across all the scanning range of the proposed system (31.25 µm), capturing one image for each $\Delta P_L = 0.335\ D$, which corresponds to an axial shift of ~ 0.5 µm. The results are shown in Fig. 10 for six different object planes. The images were processed by applying a simple thresholding to remove the out-of-focus blur. Despite the basic image processing, the images show good optical sectioning capability of the system.

Optics EXPRESS

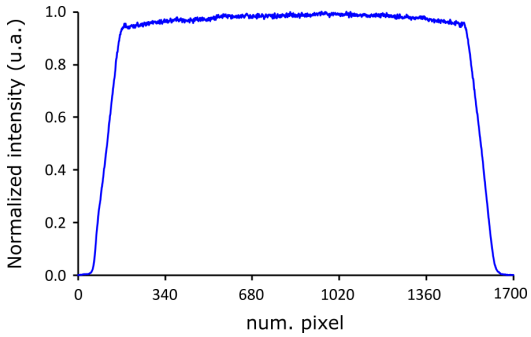

Fig. 9. Averaged normalized intensity across the FOV of the EDOF microscope.

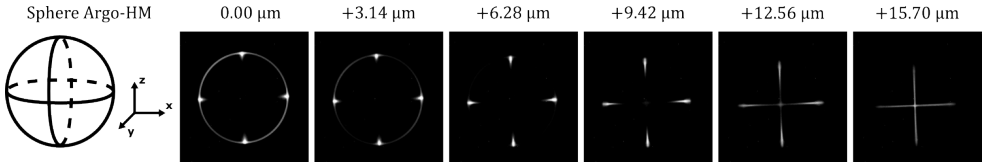

Fig. 10. The sample "Sphere" of the Argo-HM test from Argolight. The leftmost figure is a representation of the object. The remaining images (with black background) are captured with EDOF microscope mounted in the Nikon commercial microscope. Each image is captured varying the P_L to change the object plane to the distance indicated on top (z of Eq. (14)) and subsequently processed by applying a simple intensity threshold.

Finally, we tested the add-on device imaging a fixed 3D sample, consisting of yeast diluted in a solution of water and gelatin. The sample was observed with two different illumination techniques and the corresponding objectives. First, brightfield illumination was used, with a 10× / 0.45 objective (CFI Plan Apochromat λD 10×). Subsequently, the same sample was observed

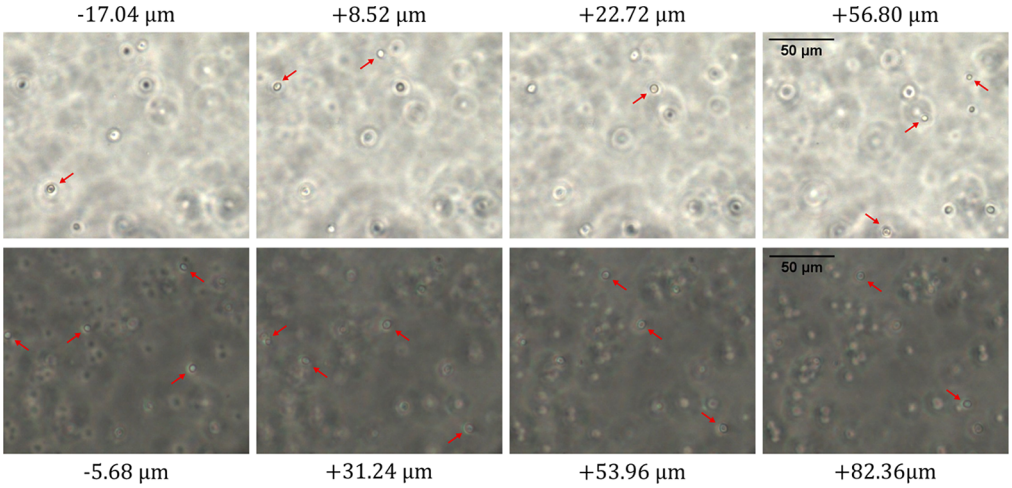

Fig. 11. Yeast fixed sample captured with the EDOF microscope mounted on the Nikon commercial microscope. Top row: the sample observed in brightfield mode focused at different depths. Bottom row: the sample observed in phase contrast microscopy focused at different depths. The red arrows indicate the focused cells at each depth.

Optics EXPRESS

through phase contrast microscopy and imaged with a 10× / 0.25 objective (CFI Achro ADL 10×F). Two complete focal stacks were acquired, varying P_L between −5 D and +15 D. As the focal length of the 10× objective is twice that of the 20× objective, the axial range in this case is 4 times higher (Eq. (14)). Figure 11 shows the detail of some of the images captured at different depths. The top row corresponds to the brightfield images, while the bottom row shows the phase contrast images. For each image, the depth is indicated relative to the native microscope object plane. For both sets of images, the different cells that come into focus at different distances are indicated with red arrows. Note that, for the phase contrast images, the worse image quality is due to the lower NA of the objective.

6. Conclusions

We have demonstrated a compact, robust and cost-effective EDOF microscope based on an ETL, to capture focal stacks of thick 3D samples. In this system, the ETL is strategically placed at the exit pupil plane, to maintain the magnification and resolution constant. We show through theoretical derivation that double-telecentric configuration is not a necessary condition for constant magnification. Therefore, to avoid alignment issues, we shortened the overall system by placing the tube lens closer to the objective and using M12 lenses as relay lenses. We demonstrate that the system achieves a constant MTF across all the scanning depth range, through a precise quantitative characterisation based on the slant edge method. After building and characterising the system on the optical bench, we implemented the EDOF microscope in a standard commercial microscope, by coupling the add-on composed by the afocal relay, the ETL and the sensor to the camera port. In this way, we demonstrate the possibility of converting any commercial microscope into an EDOF system, thanks to our portable, cost-effective add-on. To show the potential of this device, we imaged different 3D samples illuminated with different techniques, which finally proves the imaging capability and flexibility of the system.

Funding. Ministerio de Ciencia, Innovación y Universidades (PID2022-137747OB-I00); European Regional Development Fund (PID2022-137747OB-I00); Generalitat Valenciana (CIPROM/2022/30); Ministerio de Universidades (MS21-141); European Commission (MS21-141).

Disclosures. The authors declare no conflicts of interest.

Data availability. Data underlying the results presented in this paper are not publicly available at this time but may be obtained from the authors upon reasonable request.

References

1. J. Mertz, "Strategies for volumetric imaging with a fluorescence microscope," Optica **6**(10), 1261–1268 (2019).
2. E. J. Botcherby, M. J. Booth, R. Juškaitis, *et al.*, "Real-time extended depth of field microscopy," Opt. Express **16**(26), 21843–21848 (2008).
3. P. Rupprecht, A. Prendergast, C. Wyart, *et al.*, "Remote z-scanning with a macroscopic voice coil motor for fast 3d multiphoton laser scanning microscopy," Biomed. Opt. Express **7**(5), 1656–1671 (2016).
4. W. J. Shain, N. A. Vickers, B. B. Goldberg, *et al.*, "Extended depth-of-field microscopy with a high-speed deformable mirror," Opt. Lett. **42**(5), 995–998 (2017).
5. L. Jin, Y. Tang, Y. Wu, *et al.*, "Deep learning extended depth-of-field microscope for fast and slide-free histology," Proc. Natl. Acad. Sci. **117**(52), 33051–33060 (2020).
6. S. Xiao, H. Gritton, H.-a. Tseng, *et al.*, "High-contrast multifocus microscopy with a single camera and z-splitter prism," Optica **7**(11), 1477–1486 (2020).
7. J. Jiang, D. Zhang, S. Walker, *et al.*, "Fast 3-d temporal focusing microscopy using an electrically tunable lens," Opt. Express **23**(19), 24362–24368 (2015).
8. Y. Nakai, M. Ozeki, T. Hiraiwa, *et al.*, "High-speed microscopy with an electrically tunable lens to image the dynamics of in vivo molecular complexes," Rev. Sci. Instrum. **86**(1), 1 (2015).
9. S. Liu and H. Hua, "Extended depth-of-field microscopic imaging with a variable focus microscope objective," Opt. Express **19**(1), 353–362 (2011).
10. Y. Qu and H. Yang, "Optical microscopy with flexible axial capabilities using a vari-focus liquid lens," J. Microsc. **258**(3), 212–222 (2015).
11. G. Lan, T. F. Mauger, and G. Li, "Design of high-performance adaptive objective lens with large optical depth scanning range for ultrabroad near infrared microscopic imaging," Biomed. Opt. Express **6**(9), 3362–3377 (2015).

Optics EXPRESS

12. Y. Chen, H. Liu, Y. Zhou, *et al.*, "Extended the depth of field and zoom microscope with varifocal lens," Sci. Rep. **12**(1), 11015 (2022).
13. C. Liu, Z. Jiang, X. Wang, *et al.*, "Continuous optical zoom microscope with extended depth of field and 3d reconstruction," PhotoniX **3**(1), 20 (2022).
14. J. M. Jabbour, B. H. Malik, C. Olsovsky, *et al.*, "Optical axial scanning in confocal microscopy using an electrically tunable lens," Biomed. Opt. Express **5**(2), 645–652 (2014).
15. F. O. Fahrbach, F. F. Voigt, B. Schmid, *et al.*, "Rapid 3d light-sheet microscopy with a tunable lens," Opt. Express **21**(18), 21010–21026 (2013).
16. M. Duocastella, G. Sancataldo, P. Saggau, *et al.*, "Fast inertia-free volumetric light-sheet microscope," ACS Photonics **4**(7), 1797–1804 (2017).
17. M. Dal Maschio, A. M. De Stasi, F. Benfenati, *et al.*, "Three-dimensional in vivo scanning microscopy with inertia-free focus control," Opt. Lett. **36**(17), 3503–3505 (2011).
18. M. Martinez-Corral, P.-Y. Hsieh, A. Doblas, *et al.*, "Fast axial-scanning widefield microscopy with constant magnification and resolution," J. Disp. Technol. **11**(11), 913–920 (2015).
19. L. Mazzella, T. Mangeat, G. Giroussens, *et al.*, "Extended-depth of field random illumination microscopy, edf-rim, provides super-resolved projective imaging," Light: Science & Applications **13**(1), 285 (2024).
20. R. Zhang, N. Zhou, H. Tang, *et al.*, "High-speed multi-modal extended depth-of-field microscopy with an electrically tunable lens," Laser & Photonics Reviews **18**(4), 2300770 (2024).
21. L. Galdon, J. Garcia-Sucerquia, G. Saavedra, *et al.*, "Resolution limit in opto-digital systems revisited," Opt. Express **31**(2), 2000–2012 (2023).
22. M. Martinez-Corral and B. Javidi, "Fundamentals of 3d imaging and displays: a tutorial on integral imaging, light-field, and plenoptic systems," Adv. Opt. Photonics **10**(3), 512–566 (2018).
23. F. Mugele and J.-C. Baret, "Electrowetting: from basics to applications," J. Phys.: Condens. Matter **17**, R705 (2005).
24. X. Song, H. Zhang, D. Li, *et al.*, "Electrowetting lens with large aperture and focal length tunability," Sci. Rep. **10**(1), 16318 (2020).
25. F. Van den Bergh, "Robust edge-spread function construction methods to counter poor sample spacing uniformity in the slanted-edge method," JOSA A **36**(7), 1126–1136 (2019).